PTV measurements in the wake of a car side-view mirror model for validating CFD models

Canale, Christian; Arpino, Fausto; Cortellessa, Gino; Dell'isola, Marco; Grossi, Giorgio; Sciacchitano, Andrea

DOI
10.1615/ComputThermalScien.2025058350

Publication date
2025

Document Version
Final published version

Published in
Computational Thermal Sciences

PTV MEASUREMENTS IN THE WAKE OF A CAR SIDE-VIEW MIRROR MODEL FOR VALIDATING CFD MODELS

Christian Canale,[1] Fausto Arpino,[1] Gino Cortellessa,[1] Marco Dell'Isola,[1] Giorgio Grossi,[1] & Andrea Sciacchitano[2,*]

[1]*Department of Civil and Mechanical Engineering, University of Cassino and Southern Lazio, Cassino, FR, Italy*

[2]*Department of Aerospace Engineering, TU Delft, Delft, The Netherlands*

*Address all correspondence to: Dr. Andrea Sciacchitano, Department of Aerospace Engineering, TU Delft, Delft, The Netherlands; Tel.: +31 15 27 88692; Fax: +31 15 27 87077, E-mail: A.Sciacchitano@tudelft.nl

Particle-laden turbulent flows occur in various natural and industrial processes, highlighting the need for a comprehensive understanding of the interaction between the dispersed phase and the carrier flow. This study investigates the fluid dynamics of a simplified car side-view mirror model, experimentally analyzed using the particle tracking velocimetry technique in the laboratories of Delft University of Technology. Experimental measurements are used to validate a computational fluid dynamics model developed in the OpenFOAM environment. The overall objective of the research is to establish a benchmark for validating Eulerian–Lagrangian numerical models in terms of both flow dynamics and particle trajectories. In this study, the validation is limited to the Eulerian fields; validation of the discrete-phase modeling will be addressed in future work.

KEY WORDS: *Lagrangian particle tracking, computational fluid dynamics, side mirror aerodynamic*

1. INTRODUCTION

Particle-laden turbulent flows are encountered in several engineering, chemical, and environmental applications (Pei et al., 2024; Yan et al., 2024; Yang et al., 2017). Although many studies have advanced the field by developing empirical correlations based on case studies, a thorough investigation of the local flow characteristics governing the overall behavior is still needed. From a research perspective, two aspects are particularly relevant: how suspended particles affect turbulence and how they are dispersed within turbulent flows; both aspects are closely linked to the dynamics and behavior of particle-laden turbulent flows. Despite the research done through both experimental and numerical approaches, achieving a comprehensive description of the underlying physics and mechanisms remains challenging. This difficulty arises from the involvement of several nondimensional parameters, including the particle Reynolds number Re_p, particle Stokes number St_p, particle volume fraction Φ_l, particle-to-fluid density ratio ρ_r, and particle-to-turbulence length-scale ratio (Saber et al., 2015).

Computational fluid dynamics (CFD) can serve as a highly effective tool for predicting local behavior in flows containing dispersed particles. Despite its strengths, difficulties remain in setting up multiphase simulations accurately and in selecting the most appropriate modeling approach to capture the intricate interactions between phases. Particle transport in such flows is inherently complex and plays a crucial role in a wide range of practical applications, such as controlling emissions in the automotive sector, maintaining indoor air quality, and understanding how airborne pollutants spread in occupied spaces (Arpino et al., 2022a,b, 2023; Poelma et al., 2007; Weil et al., 1992). Establishing a dependable predictive framework is essential for enhancing the accuracy and efficiency of prototype assessments in these scenarios. Several studies have explored different approaches to analyzing particle-laden flows. For instance,

Submitted: 1/31/2025; Accepted: 6/14/2025; Online: 7/9/2025 https://doi.org/10.1615/ComputThermalScien.2025058350

NOMENCLATURE

H	side-view mirror model height (m)	ρ_r	particle-to-fluid density ratio
k	turbulent kinetic energy (m^2s^2)	Φ_V	particle volume fraction
L	characteristic length (m)	$\boldsymbol{\omega}$	specific rate of dissipation (s^{-1})
ℓ	turbulent mixing length (m)	**Abbreviations**	
$\boldsymbol{n}$	unit surface normal vector	CFD	computational fluid dynamics
n_i	number of data points	HFSB	helium-filled soap bubbles
p	pressure (Pa)	LED	light-emitting diode
Re	Reynolds number	PIV	particle image velocimetry
St	Stokes number	PTU	programmable time unit
t	time (s)	PTV	particle tracking velocimetry
$\boldsymbol{u}$ (u, v, w)	velocity ($m \cdot s^{-1}$)	STB	shake-the-box
x, y, z	Cartesian directions		
Greek Symbols		**Subscripts**	
δ	boundary layer height (m)	p	particle
μ	dynamic viscosity (Pa s)		
μ_t	turbulent viscosity (Pa s)	**Superscripts**	
ρ	density ($kg\ m^{-3}$)	–	time-averaged quantity

Kim et al. (2020) investigated the fluid dynamics of various side mirror geometries using the particle tracking velocimetry (PTV) technique to evaluate three distinct configurations. Elhimer et al. (2017) introduced an innovative technique for simultaneous particle velocity measurements in a three-dimensional turbulent flow, comparing results from particle image velocimetry (PIV) and PTV. Additionally, Chen (2009) conducted numerical simulations to assess the performance of ventilation systems in indoor environments, aiming to identify the most effective CFD approach for particle dispersion analysis.

In this study, an experimental campaign using the PTV technique was conducted to examine particle-laden flow around a car side-view mirror model. Although this research has direct relevance to automotive applications, the setup also serves as a benchmark study due to its well-defined boundary conditions and replicable experimental configuration. The primary objective is to establish a consistent benchmark case for the validation of a Eulerian–Lagrangian model for both the continuous and discrete phases, ensuring the reliability of numerical simulations not only for airflow dynamics but also for particle trajectories. This research is ongoing, and the findings presented here are focused on experimental analyses using helium-filled soap bubbles (HFSB), as well as the validation of Eulerian fields predicted by CFD simulations carried out in the OpenFOAM environment.

2. MATERIALS AND METHODS

2.1 Experimental Campaign

The experimental campaign to investigate the fluid dynamics of the side-view mirror model was conducted in the W-Tunnel at the Aerodynamics Laboratories of Delft University of Technology, the Netherlands. This open jet wind tunnel features a contraction ratio of 1:4, a square exit measuring 0.4 × 0.4 m, and a maximum achievable velocity of ≈ 35 m/s. Figure 1 illustrates the experimental setup, where the side-view mirror model is mounted on a black-covered supporting plate with dimensions of 1 m × 0.8 m × 0.01 m. The plate is placed 0.4 m downstream of the W-Tunnel exit

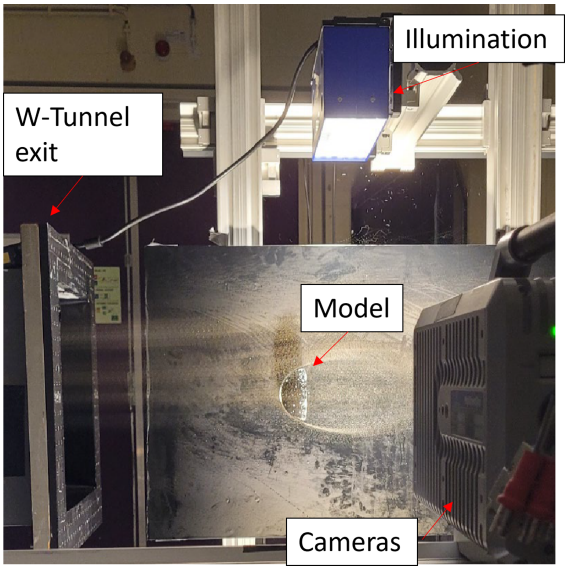

FIG. 1: Experimental setup for measurements conducted in the W-Tunnel of Delft University of Technology

and is vertically centered relative to the tunnel exit. To minimize flow separation on impact with the supporting plate, its edges were beveled at an angle of 45°.

The velocity field was measured both upstream and downstream of the model using the three-dimensional PTV technique. The side-view mirror model was immersed in the turbulent boundary layer, where the boundary layer height δ relative to the model height H was approximately $\delta/H \approx 0.2$. The experimental conditions are summarized in Table 1, with the model height serving as the characteristic length for the Reynolds number (Re_H).

The dimensions of the measurement volume were 0.3 m × 0.3 m × 0.3 m. To achieve a comprehensive understanding of the flow behavior, the measurement session was divided into two phases: an upstream study focusing on the potential flow and a downstream study analyzing the wake. During the transition from upstream to downstream measurements, the model's position was kept fixed. Instead, the measurement system was translated accordingly to maintain consistent optical and magnification properties, as well as to preserve the flow dynamics around the model. Figure 2 shows the side-view mirror model analyzed in the W-Tunnel. It consists of a half-cylinder with a quarter-sphere mounted on top, representing one of the simplest configurations studied in automotive aerodynamics (Fu and Li, 2023; Kim et al., 2020). This design was selected to generate a dataset that is both valuable to the scientific community and easily replicable under the specified boundary conditions.

2.2 Measurement System

Four high-speed cameras were positioned 0.7 m from the measurement volume. These cameras were mounted on a beam structure, allowing for seamless movement without affecting the imaging characteristics. This setup ensured

TABLE 1: Experimental conditions

Freestream velocity	10 m/s
Re_H	66,027
Model's height	10 cm
Model's width	5 cm
Blockage ratio	1.4%

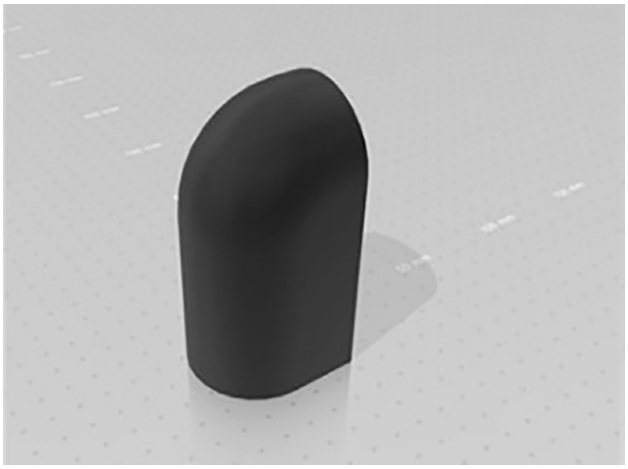

FIG. 2: Side-view mirror model employed in the PTV measurements

consistent image quality when transitioning from upstream to downstream measurement domains. To achieve uniform illumination and prevent shadowing, two light-emitting diodes (LEDs) were placed at the top and bottom of the model. A programmable time unit (PTU) was linked to a personal computer, the imaging systems, and the LED units to ensure synchronization during data acquisition. Neutrally buoyant HFSB were used as flow tracers due to their larger scattering cross-section compared with conventional micrometric particles. The tracer particles had a nominal diameter of 300 μm, with a maximum expected dispersion of 50 μm, as reported by Faleiros et al. (2019). For a detailed description of the HSFB rake characteristics, see Kim et al. (2020). Table 2 summarizes the main experimental parameters, including the optics and imaging specifications of the four cameras, as well as the illumination settings.

Table 3 outlines the characteristics of the seeding rake of the HFSB. The high scattering efficiency of HFSB enabled the use of a low-energy light source, as detailed in Table 2. However, due to the specific configuration of the experimental domain, the raw images exhibited some scattering zones, which were mitigated by applying a subtime filter to the time history of pixel intensity. The resulting images were then analyzed using the shake-the-box (STB) algorithm implemented in LaVision *DaVis* 10. With an acquisition frequency of 5.4 kHz, a particle moving at a freestream velocity of 10 m/s traveled approximately 2 mm between frames, ensuring accurate flow tracking. The instantaneous data was then averaged in space and time within 13.4-mm bins with 75% overlap, resulting in a vector pitch of 3.4 mm.

TABLE 2: Optics and imaging specifications of the four cameras and illumination settings

		Cameras 1–3	**Camera 4**
Optics	Focal length (mm)	60	50
	f#	24	28
Imaging	Model	Photron Fastcam SA1.1	Photron Fastcam SA-X2
	Pixel size (μm × μm)	20 × 20	
	Acquisition frequency (Hz)	5400	12,500
	Magnification factor	0.082	
Illumination	Pulse energy	25 mJ	
	Wavelength	527 nm	
	Spread angle	40°	

TABLE 3: Characteristics of the seeding rake used for the experimental session with HFSB

Number of nozzles	200
Nominal diameter of particles	300 μm
Production rate	$2 \cdot 10^6$
Time response of particles	$1 \cdot 10^{-5}$ s

2.3 Numerical Model

In the present study, numerical analyses were limited to evaluating the Eulerian fields without simulating the presence of particles. Future developments of this activity will focus on fully resolving the particle-laden flow evolving in the experimental scenario using a Eulerian–Lagrangian model. With this approach, the air (representing the continuous phase) will be described using a Eulerian approach by solving mass and momentum conservation equations (Versteeg and Malalasekera, 2007); the motion of particles (the discrete phase) will be tracked by solving Newton's second law (Arpino et al., 2022a,b).

Simulations were performed using the open-source OpenFOAM toolbox, which employs a finite volume formulation. The flow was assumed to be unsteady, incompressible and turbulent. Turbulence effects were modeled using the unsteady Reynolds-averaged Navier–Stokes (URANS) approach, and specifically the shear stress transport (SST) k–ω model. According to the modelling assumptions, mass and momentum conservation equations read as follows:

$$\nabla \cdot (\overline{\boldsymbol{u}}) = 0 \tag{1}$$

$$\frac{\partial \overline{\boldsymbol{u}}}{\partial t} + \nabla \cdot (\overline{\boldsymbol{u}}\overline{\boldsymbol{u}}) = -\frac{1}{\rho}\left(\nabla \overline{p} + \frac{2}{3}\rho \nabla k\right) + \nabla \cdot \left[\frac{1}{\rho}(\mu + \mu_t)\nabla \overline{\boldsymbol{u}}\right]. \tag{2}$$

Further details of the URANS turbulence model are available in Hanjalić et al. (2003).

The pressure-velocity coupling was handled with the Pressure Implicit with Splitting of Operators (PISO) algorithm, enabling the processing of fully transient phenomena with a real-time step (Greenshields and Weller, 2022). The time step size was determined based on a maximum Courant–Friedrichs–Lewy (CFL) number of 2 (Arpino et al., 2022a).

Although the simulations were fully transient, time-averaged fields were used for experimental-numerical comparison. To define the averaging start time, six virtual probes were placed within the computational domain both upstream and downstream of the model. After a 4-s simulation, the velocity deviation at these locations dropped below 1.5%, and time-averaging was performed over the following 10 s. The computational domain is shown in Fig. 3, and the complete list of boundary conditions is provided in Table 4. The turbulent mixing length ℓ was calculated as the 7% of the model width, representing the characteristic length L.

The computational grid was generated with the *snappyHexMesh* algorithm, and the mesh size was established according to a grid sensitivity analysis; velocity fields predicted with three grids were compared (Table 5). In particular, velocity profiles at two sections were compared: on the stagnation streamline (as depicted in Fig. 4a) and over the top surface of the side-view mirror model (Fig. 4b).

Results of the grid sensitivity analysis are reported in Table 6 in terms of average errors, calculated taking the Mesh 3 (i.e., the finest) as reference, according to the following expression:

$$error = \frac{1}{n_i}\sum_{i=1}^{n_i} \frac{\left|u_{mesh_j,i} - u_{mesh_3,i}\right|}{u_{mesh_3,i}} \tag{3}$$

where $u_{mesh_j,i}$ is the velocity magnitude predicted with mesh j at point i, and n_i represents the number of extracted data points.

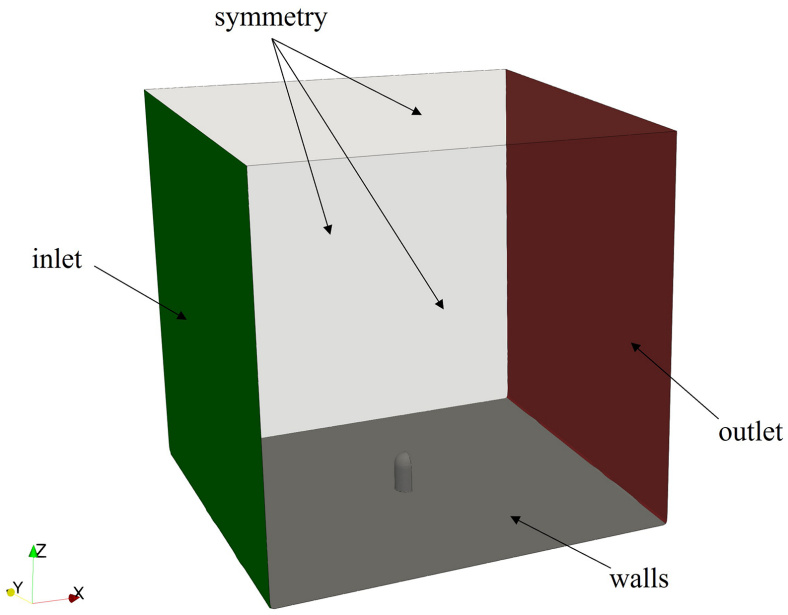

FIG. 3: Computational domain employed for numerical simulations

TABLE 4: Boundary conditions set for the numerical model validation

Surface	BC for velocity	BC for pressure	BC for k	BC for ω
Inlet	$u = 10\ m \cdot s^{-1}$	$\partial p/\partial \boldsymbol{n} = 0$	$\boldsymbol{k} = 0.1\ m^2 \cdot s^{-2}$	$\ell = 0.07\ L$
Outlet	$\partial \boldsymbol{u}/\partial \boldsymbol{n} = 0$	$p = 0$	$\partial k/\partial \boldsymbol{n} = 0$	$\partial \omega/\partial \boldsymbol{n} = 0$
Symmetry	Symmetry			
Walls	$\boldsymbol{u} = 0$	$\partial p/\partial \boldsymbol{n} = 0$	Standard wall functions	

TABLE 5: Characteristics of the three meshes used for the sensitivity analysis

	Mesh 1	Mesh 2	Mesh 3
Number of cells	$1.21 \cdot 10^6$	$2.08 \cdot 10^6$	$4.46 \cdot 10^6$
Maximum skewness	0.96	0.96	0.97
Average nonorthogonality	37.24	36.92	36.66

Because the average error between mesh 2 and mesh 3 was below 5%, the former was selected for numerical analyses. A clipped view of the selected grid is provided in Fig. 5; as shown, a refinement box in the proximity of the side-view mirror model was generated, to describe the boundary layer development and separation resulting from the interaction of the incoming flow with the side-view mirror model.

3. RESULTS

3.1 Experimental Results

The fluid dynamics of the side-view mirror model were analyzed in terms of time-averaged velocity fields. Figure 6 displays the time-averaged streamwise velocity contours within the x–z plane at y = 0. The flow accelerates above the

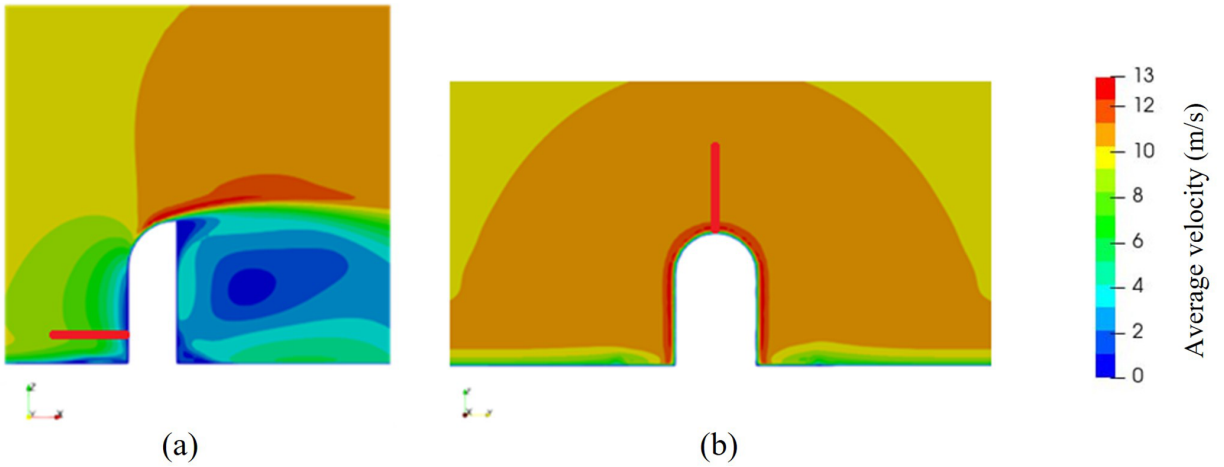

FIG. 4: Predicted mean velocity contours on the (a) x–z and (b) y–z planes crossing the side-view mirror model at its midpoint, along with the extraction lines for velocity profiles comparison along x and z directions

TABLE 6: Results of the grid sensitivity analysis

	Error mesh 1–3	Error mesh 2–3
x-profile	8.2%	3.5%
z-profile	3.4%	0.9%

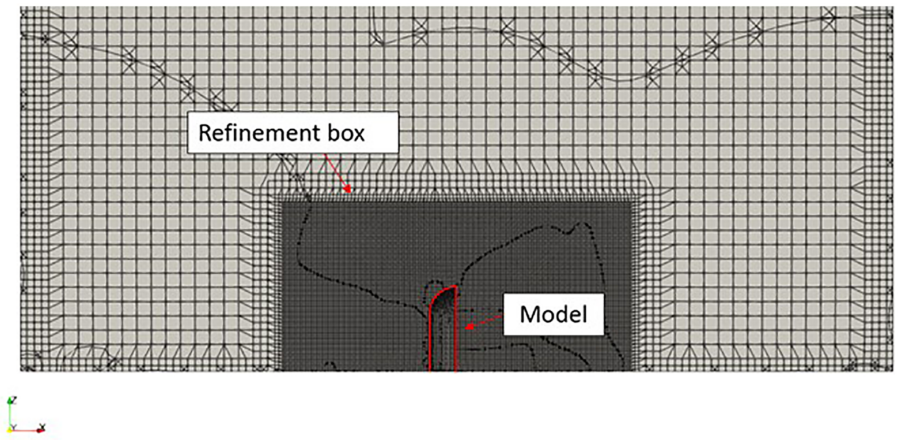

FIG. 5: Clipped view of the computational grid selected as a result of the sensitivity analysis

main recirculation region due to the blockage induced by the wake, as visible in the orange zone above the side-view mirror model. To assess the uncertainty in the mean velocity measurements, Davis software was used; the evaluation considered the instantaneous velocity components, and the maximum standard deviation of the velocity component was determined to be 0.14 m/s. Following Sciacchitano and Wieneke (2016), the uncertainties of the time-averaged velocity components were computed as follows:

$$U_{\bar{u}} = \frac{k\sigma_u}{\sqrt{N}},$$

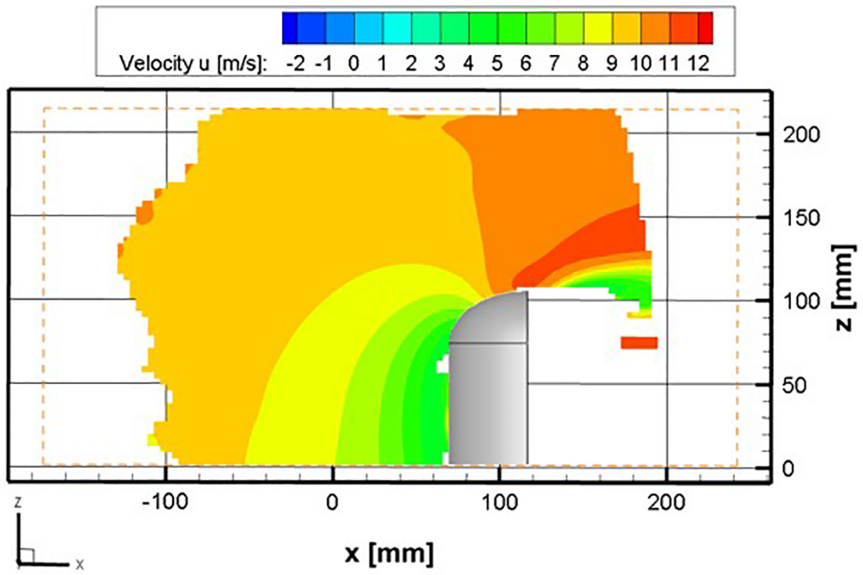

FIG. 6: Experimental x-velocity contours on the x–z slice crossing the side-view mirror model at its midpoint

where k is the coverage factor, set equal to 1.96 for 95% confidence level, σ_u is the local standard deviation of the velocity component, and N is the number of tracks in a bin. Consequently, the uncertainty in the mean flow component within the turbulent wake region is defined with a 1.4% margin for a single measurement at a freestream velocity of 10 m/s.

3.2 Comparison with Numerical Results

Comparison of experimental and numerical results was performed in two stages. First, using the extraction lines defined in Fig. 4, a comparison of the average velocity field was performed. The results, presented in Fig. 7, indicate a reasonable agreement between simulations and experiments, despite the discrepancies observed in the regions close to the side-view mirror model; in particular, for the x-profile (Fig. 7a), the error is equal to 54.56% at x = 55 mm with an average of 7.96%. The reason the discrepancy between the CFD and the PTV results increases along the stagnation streamline is that the tracer particles were not perfectly neutrally buoyant but slightly heavier than air; because of their higher density, they experience a delayed deceleration with respect to the surrounding flow, as reported in Scarano et al. (2015). This effect is negligible in most of the flow field, but it is visible along the stagnation streamline because it accumulates over time, resulting in a particle trajectory that departs from the stagnation streamline in proximity of the stagnation point. Regarding the z-profile (Fig. 7b), the average error is equal to 2.53%, with a maximum error of 24% at z = 103 mm. The overall average error is equal to 4.56%, which is consistent with the measurement uncertainties.

An additional comparison is provided in Fig. 8, which illustrates the superimposition of experimental and numerical isolines of the average velocity for the upstream region. In this visualization, black lines represent the experimental isolines, whereas numerical data are colored according to velocity. The strong agreement between the two fields, as evident from the isoline comparison, highlights the accuracy of the numerical model in capturing key flow characteristics. Furthermore, the low average error previously discussed reinforces the model's reliability, validating its ability to reproduce the experimental data with an acceptable degree of precision.

4. CONCLUSIONS

The present research is part of a preliminary study on the fluid dynamics of a side-view mirror model, with measurements conducted in a wind tunnel facility of the Delft University of Technology laboratories. The experimental work

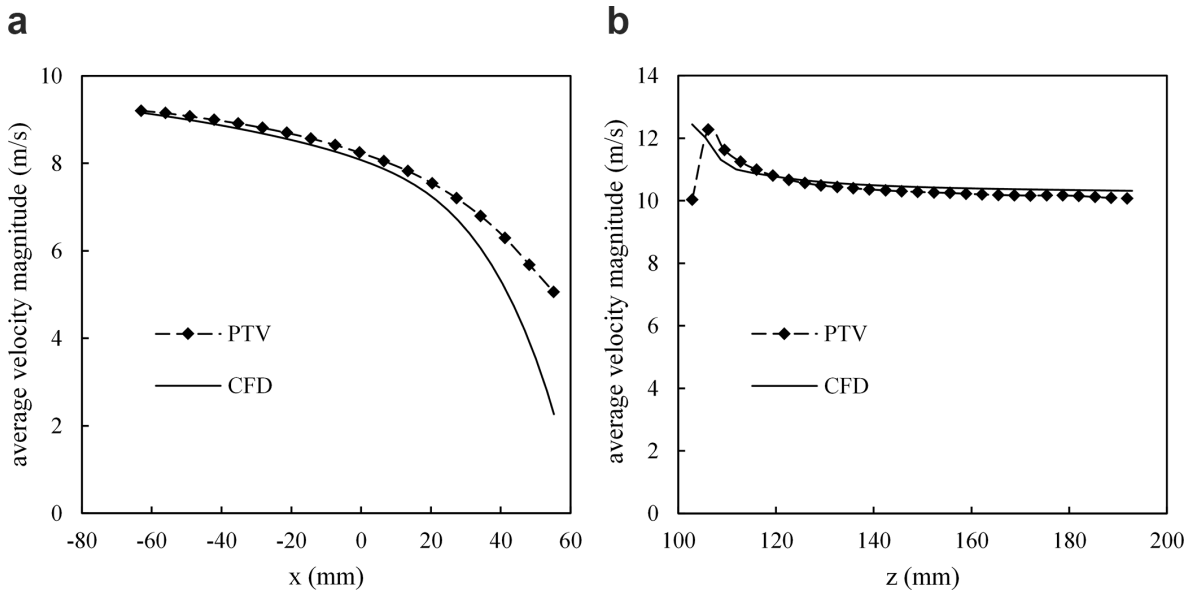

FIG. 7: Experimental-numerical comparison along the (a) x-axis and (b) z-axis at the center of the side-view mirror model, at y = 0

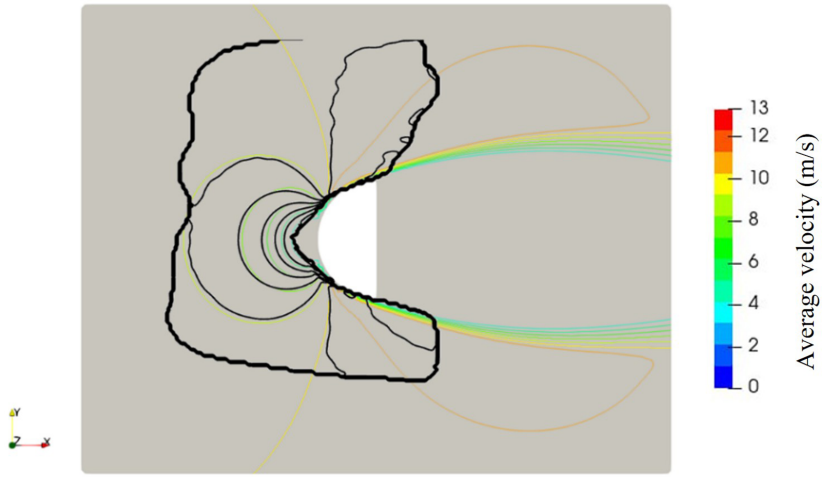

FIG. 8: Comparison of the isolines of the average velocity around the side-view mirror model between experiments (black) and simulations (colored)

aimed to generate a dataset useful for studying a simplified model with easily replicable boundary conditions and setup characteristics. A PTV methodology was employed using the STB algorithm, with four high-speed cameras and HFSB as tracers in wind tunnel experiments. Additionally, the study aimed to validate a CFD model describing the airflow dynamics around the experimentally investigated side-view mirror model. Future research activities will involve the development and validation of the Lagrangian CFD model to describe particle dynamics.

REFERENCES

Arpino, F., Cortellessa, G., D'Alicandro, A.C., Grossi, G., Massarotti, N., and Mauro, A., CFD Analysis of the Air Supply Rate Influence on the Aerosol Dispersion in a University Lecture Room, *Build. Environ.*, vol. **235**, p. 110257, 2023.

Arpino, F., Cortellessa, G., Grossi, G., and Nagano, H., A Eulerian–Lagrangian Approach for the Non-Isothermal and Transient CFD Analysis of the Aerosol Airborne Dispersion in a Car Cabin, *Build. Environ.*, vol. **209**, p. 108648, 2022a.

Arpino, F., Grossi, G., Cortellessa, G., Mikszewski, A., Morawska, L., Buonanno, G., and Stabile, L., Risk of SARS-CoV-2 in a Car Cabin Assessed through 3D CFD Simulations, *Indoor Air*, vol. **32**, no. 3, 2022b.

Chen, Q., Ventilation Performance Prediction for Buildings: A Method Overview and Recent Applications, *Build. Environ.*, vol. **44**, no. 4, pp. 848–858, 2009.

Elhimer, M., Praud, O., Marchal, M., Cazin, S., and Bazile, R., Simultaneous PIV/PTV Velocimetry Technique in a Turbulent Particle-Laden Flow, *J. Vis.*, vol. **20**, no. 2, pp. 289–304, 2017.

DaVis Software. Available from: https://www.lavision.de/en/products/davis-software/.

Faleiros, D.E., Tuinstra, M., Sciacchitano, A., and Scarano, F., Generation and Control of Helium-Filled Soap Bubbles for PIV, *Exp. Fluids*, vol. **60**, no. 3, p. 40, 2019.

Fu, W. and Li, Y., Experimental Study on a Generic Side-View Mirror with Slotted Cylindrical Foot, *J. Appl. Fluid Mech.*, vol. **16**, no. 2, pp. 363–374, 2023.

Greenshields, C.J. and Weller, H.G., *Notes on Computational Fluid Dynamics: General Principles*, Reading, United Kingdom: CFD Direct Limited, 2022.

Hanjalić, K., Nagano, Y., and Tummers, M.J., Eds., *Turbulence, Heat and Mass Transfer 4: Proceedings of the Fourth International Symposium on Turbulence, Heat and Mass Transfer*, Antalya, Turkey, 12–17 October, 2003, New York, NY: Begell House, 2003.

Kim, D., Kim, M., Saredi, E., Scarano, F., and Kim, K.C., Robotic PTV Study of the Flow around Automotive Side-View Mirror Models, *Exp. Therm. Fluid Sci.*, vol. **119**, p. 110202, 2020.

Pei, Y., Chen, W., Xiong, X.-L., Xu, X., and Zhou, Y., Direct Numerical Simulation of Turbulent Flow and Heat Transfer in a Particle-Laden Turbulent Channel Flow, *Int. J. Heat Fluid Flow*, vol. **110**, p. 109617, 2024.

Poelma, C., Westerweel, J., and Ooms, G., Particle–Fluid Interactions in Grid-Generated Turbulence, *J. Fluid Mech.*, vol. **589**, pp. 315–351, 2007.

Saber, A., Lundström, T.S., and Hellström, J.G.I., Turbulent Modulation in Particulate Flow: A Review of Critical Variables, *Engineering*, vol. **7**, no. 10, pp. 597–609, 2015.

Scarano, F., Ghaemi, S., Caridi, G.C.A., Bosbach, J., Dierksheide, U., and Sciacchitano, A., On the Use of Helium-Filled Soap Bubbles for Large-Scale Tomographic PIV in Wind Tunnel Experiments, *Exp. Fluids*, vol. **56**, no. 2, p. 42, 2015.

Sciacchitano, A. and Wieneke, B., PIV Uncertainty Propagation, *Measure. Sci. Technol.*, vol. **27**, no. 8, p. 084006, 2016.

Versteeg, H.K. and Malalasekera, W., *An Introduction to Computational Fluid Dynamics: The Finite Volume Method*, Harlow, United Kingdom: Pearson Education Ltd., 2007.

Weil, J.C., Sykes, R.I., and Venkatram, A., Evaluating Air-Quality Models: Review and Outlook, *J. Appl. Meteorol.*, vol. **31**, no. 10, pp. 1121–1145, 1992.

Yan, Y., Mortimer, L.F., Wolde, B., Fairweather, M., Zhao, Y., and Yao, J., Effect of Secondary Flow and Wall Collisions on Particle-Laden Flows in 90° Pipe Bends, *Int. J. Multiphase Flow*, vol. **179**, p. 104925, 2024.

Yang, K., Zhao, L., and Andersson, H. I., Preferential Particle Concentration in Wall-Bounded Turbulence with Zero Skin Friction, *Phys. Fluids*, vol. **29**, no. 11, p. 113302, 2017.